

Use of MEMS Gyroscopes in Active Vibration Damping for HSM-driven Positioning Systems

Riccardo Antonello, Angelo Cenedese and Roberto Oboe
University of Padova

Department of Management and Engineering, Vicenza, Italy

Email: {riccardo.antonello, angelo.cenedese, roberto.oboe}@unipd.it

Phone: +39-0444-998844; Fax: +39-0444-998888

Abstract—Hybrid Stepper Motors (HSM) are the workhorses in many low-end motion control systems, given their low cost and high reliability. The resolution of the positioning systems using this type of motors has been increased with the introduction of the microstepping driving technique, even if, being operated in open loop, HSM cannot provide the actual control of the load position. Recently, the authors have proposed an innovative control scheme [1], based on the use of a load side acceleration sensor, that implements the active damping of a HSM-driven mechanical load, in presence of a flexible mechanical transmission between motor and load. This is a typical industrial scenario, in which the problem of the oscillations arising from the excitation of the mechanical resonance by various disturbances (including torque ripple) is usually addressed by severely limiting the overall dynamic performance. In this paper, we propose the extension of the proposed technique, with the use of a MEMS gyroscope to implement an active damping control strategy, which allows for the improvement of the dynamic response and an excellent rejection of the oscillations caused by the torque ripple. The proposed technique does not require the re-design of the existing equipments, since it is based on the real time modulation of the orientation of the stator flux, aimed at producing a compensating torque and, in turn, damping the oscillatory modes. Experimental results, obtained with a HSM-driven camera positioning unit, confirm the effectiveness of the proposed solution.

I. INTRODUCTION

Hybrid Stepper Motors (HSM) are used in many low-end motion control applications, where the cost constraints are traded with a limited level of performance. This type of motor works as a stepping motor by the combined principles of the permanent-magnet motor and the variable reluctance motor [2]. The particular toothed structure of the stator (with the same pitch of the rotor), allows steps with the width of a quarter of a teeth, when the two phases of the stator windings are driven in an on/off fashion (see Fig. 1). HSMs driven in such a way share with all other stepper motors the problem of a non-smooth torque generation, together with an oscillatory behavior in step-to-step motion. A widely applied driving technique that partially alleviates the above problems, is the so-called microstepping [3], in which the phase currents are two sinusoids in quadrature (see Fig. 2). With this driving technique, the stator flux rotates smoothly, thus limiting torque ripple and rotor oscillations.

It is well known, however, that even with the use of microstepping, torque ripple cannot be avoided, especially due to the presence of a large detent torque [4] [5] [6]. This fact has

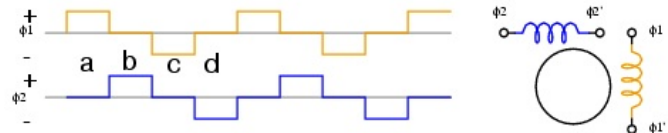


Fig. 1. Square wave driving of 2-phase stepper motor.

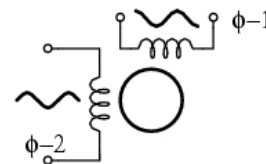


Fig. 2. Microstepping: sinusoidal driving of 2-phase stepper motor.

often prevented the application of HSMs in all those systems in which mechanical resonances could amplify the effects of torque ripple, resulting in large load oscillations. Indeed, several authors have proposed complex ripple minimization techniques, but all of them require a rotor position sensor, thus vanishing the cost benefit of having an open loop position actuator [4] [7] [8].

Vibration suppression and control in mechanical loads with resonant modes is a widely studied subject and several practical and effective solutions have been found, like input shaping and active damping [9]. The input shaping techniques, however, are best suited for point-to-point motions, and they do not provide any remedy against the load oscillations due to disturbances, like torque ripple, always present in HSMs. Active damping has found a notable application in the control of flexible structures, and it has been implemented either by distributing damping actuators along the structure to be controlled (e.g. piezoelectric actuators on the modal nodes of an elastic beam) or, in case a single actuator is available, by properly controlling the generated torque. In principle, the idea is simple: inject a force/torque, equivalent to that produced by a viscous damper, to reduce the amplitude of the vibrations, caused either by disturbances or transients in point-to-point motions. This idea, of course, has a straightforward application in all those systems provided by a torque-controllable actuator (e.g. DC motor, AC brushless motors etc.), but it has some

implementation hurdles in position controlled actuators, like HSMs.

In a previous paper, the authors proposed the application of an active damping technique to a system with mechanical resonances and driven by a HSM [1]. It has been shown that it is possible to generate a torque for the compensation of the oscillatory behavior by using a phase modulation of the currents applied to the stator windings. The modulation, in turn, was driven by the velocity of the load, obtained by processing the output of a low-cost MEMS accelerometer. In this paper, we extend the proposed approach, by using the direct measurement of the load side angular speed, measured with a MEMS gyroscope. The paper is organized as follows. Section II briefly describes the positioning unit for surveillance camera that has been used as a case study for the application of the proposed technique. Section III highlights the main issues of the mathematical model of the system to be controlled, with some details on the factors that may lead to plant changes and, in turn to robustness problems. Section IV describes the control strategy, together with a brief description of the solution adopted to generate the damping torque. The experimental results obtained are reported in Section V, while conclusions and future research directions are presented in Section VI.

II. POSITIONING UNIT FOR SURVEILLANCE CAMERA

In order to test the feasibility of an active vibration suppression scheme, when the load is driven by a HSM, we used a positioning unit for surveillance cameras, shown in Fig. 3. This is a pan-tilt unit, with adjustable focus and zoom. In pan and tilt, the camera is moved by two HSMs, connected to the load through a reduction unit, composed of two gears and a toothed belt (Fig. 4). The motors have a step angle of 1.8° , with a holding torque of 220 Ncm, when the phase current reaches 2.8 A. The positioning unit can be controlled manually, via a user console, or automatically, with a video processing unit that commands the pan and tilt angle in order to track a moving target. It is worth noticing that most of the target tracking motion involves the control of the pan angle, while the tilt angle of the camera has a rather small variation. For this reason, in the following, the dynamic model of the plant will be defined only for the pan axis. The test unit mounts two MEMS sensors, shown in Fig. 4. The first one is an accelerometer, placed as far as possible from the center of the pan axis (this in order to maximize the sensitivity) and used to measure the tangential acceleration during plant model identification. The second sensor is a gyroscope, mounted in order to measure the pan rotational speed and actually used to get the load side velocity in the active vibration control system described in Section IV.

This unit operates outdoor, in potentially harsh environmental conditions and it can be mounted on a wide variety of supports. Additionally, it is subjected to various disturbances (ranging from wind gusts to birds hanging on the unit) and some of the operating parameters (e.g. friction of the sealing rings, stiffness of the belts, etc.) may widely change with

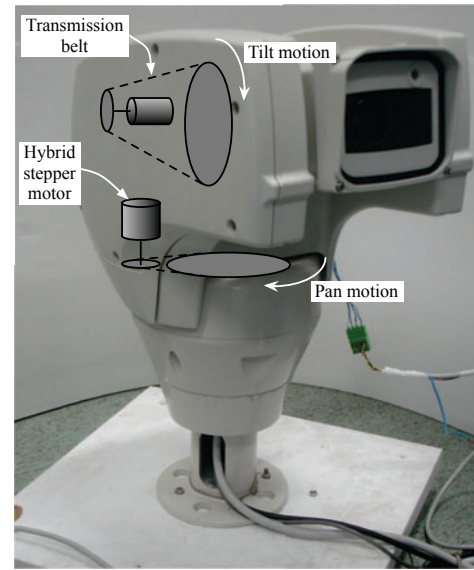


Fig. 3. Positioning unit for surveillance camera. Motors and gears positions are shown

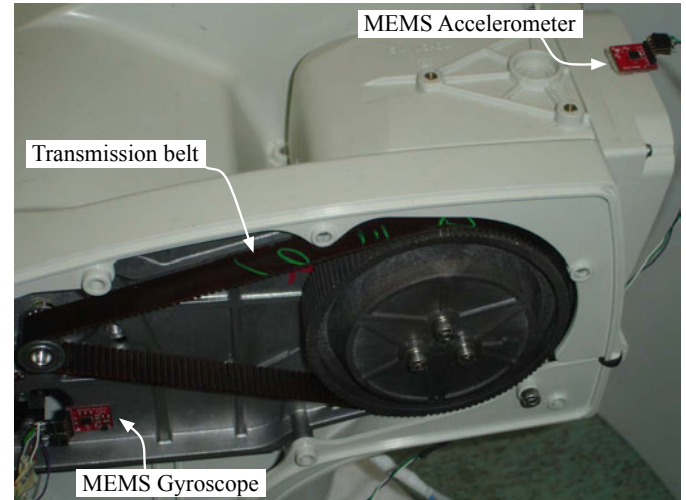


Fig. 4. Reduction unit with gears and toothed belt. MEMS sensors are also shown

the operating temperature, ranging from -40 to $+60$ centigrades. Finally, the use of elastic transmission belts leads to unavoidable mechanical resonances, which may amplify the effects of the torque ripple generated by the HSM and other disturbances.

The unit comes without a load position sensor, so the tracking of a moving target is performed simply by acting on the HSM stator flux angular position, without any feedback. Rotations of the unit at a constant angular rate $\dot{\theta}$ (e.g. when following a target moving at a constant speed) are obtained with a microstepping drive, i.e. by applying to the stator windings two quadrature sinusoidal currents with a fixed frequency $\omega = (N_r N_G) \dot{\theta}$, where N_r is the number of pole pairs of the HSM and N_G is the gear ratio. In such

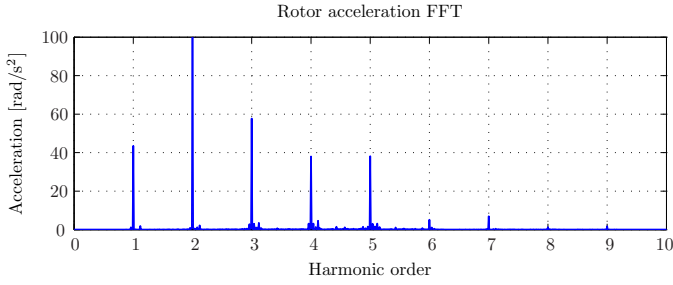


Fig. 5. Torque harmonics of the HSM.

operating conditions, the torque ripple generated by the HSM is composed of several harmonics, with a base frequency equal to that of the stator currents. Such harmonics are generated by both the driving amplifiers (which may introduce differences in offsets and amplitudes of the phase currents) and motor imperfections [10] [11]. As an example, the HSM used in moving the pan angle of the unit has a measured torque ripple spectrum as in Fig. 5, obtained by measuring the tangential acceleration of the load with the MEMS accelerometer mounted on top of the camera case.

III. ELECTRO-MECHANICAL SYSTEM MODELING

In order to properly design the active damping control of the vibrational modes for the system described in the previous section, we need to derive its analytical model, by means of which it is also possible to evaluate the effects of the variation of a single mechanical parameter, like the camera case inertia (e.g. due to a bird hanging on it or to a change in the zooming level) or the support stiffness. Secondly, we must study the torque generation mechanisms in HSMs, in order to find an effective way to inject a compensating torque in the system. In Fig. 6 we report the multibody model of the camera positioning unit, w.r.t. the pan angle θ_2 motion. The left part of the model is the fixed part of the unit (Sun), anchored to the ground through an torsional spring with elastic constant K_{base} ; the right part represents the HSM, with inertia J_{sh} . The two parts are connected via the springs K_{b1} and K_{b2} , accounting for the transmission belt elasticity.

Also, we indicate with θ_1 the relative angular displacement of the base w.r.t. the fixed structure, with θ_2 the hub rotation angle (output), with θ_{sh} the rotor field angle w.r.t. θ_2 , and with θ_u the stator field angle w.r.t. θ_2 (input).

In order to get the full model of the system, we need to define the input torque, generated by the HSM, and driving the hub rotation. It is worth noticing that, using the microstepping technique, the stator field can be oriented with an arbitrary angle θ_u , by driving the stator windings with two current in quadrature, namely $i_1 = I \cos(\theta_u)$ and $i_2 = I \sin(\theta_u)$. In absence of a load torque, the rotor aligns its magnetic axis with the stator field (i.e. $\theta_u = \theta_{sh}$). When an external load is applied, this causes a displacement between rotor and stator flux, according to

$$\tau_m = K_T I \sin(\theta_u - \theta_{sh}) \quad (1)$$

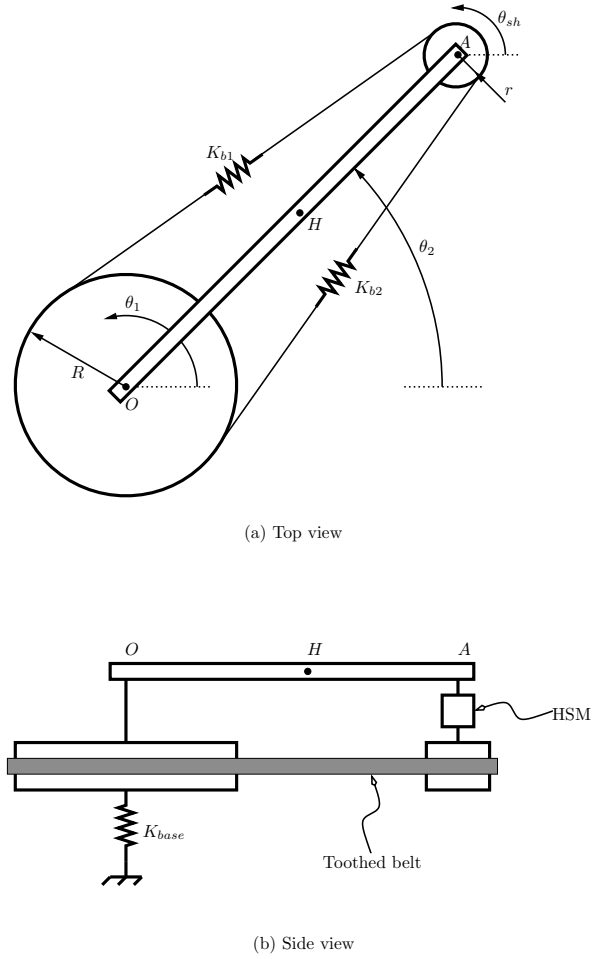


Fig. 6. Multibody model of the camera positioner.

This, in turn, can be linearized for small displacement, around the equilibrium, yielding

$$\tau_m \approx K_T I (\theta_u - \theta_{sh}) \quad (2)$$

Clearly, the above result shows that the HSM behaves like a spring, with an equivalent stiffness depending on the motor torque constant K_T and the level of the driving current I . This is a key point for the generation of the compensating torque, described later.

The next step is to derive the transfer function of the system by considering the stator flux angular position θ_u as the system input and the hub (camera) angle θ_2 as the system output. It can be proved that such transfer function has three pairs of complex conjugate poles and two pairs of complex conjugate zeros:

$$\frac{\Theta_2(s)}{\Theta_u(s)} = \frac{\prod_{k=1}^2 s^2 + 2\delta_{z_k} \omega_{z_k} s + \omega_{z_k}^2}{\prod_{k=1}^3 s^2 + 2\delta_{p_k} \omega_{p_k} s + \omega_{p_k}^2} \quad (3)$$

with $\Theta_2(s)$ and $\Theta_u(s)$ being the Laplace transforms of, respectively, the angles θ_2 and θ_u .

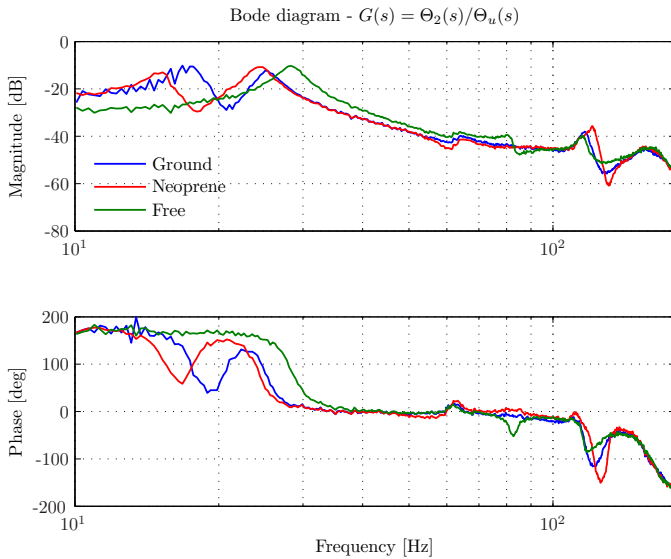


Fig. 7. Experimental frequency response $\Theta_2(s)/\Theta_u(s)$ with different support stiffnesses.

It is worth noticing that in all the above derivation, for the sake of simplicity, no difference between electrical and mechanical angle of the HSM motor has been explicitly shown, even if they have been considered in the derivation of (3). In practice, the motor used in the positioning unit has $N_r = 50$ teeth, corresponding to 1.8° of step angle. As for the ratio between motor and load position, it is $N_G = \theta_2/\theta_u = 1/7$.

We identified experimentally the frequency response of the actual system, by using both a sweep signal and a filtered white noise as a driving signal θ_u . To measure the load motion during identification, we used the MEMS accelerometer (Analog Device ADXL-335 3-axis, with $3.6g$ full scale range), placed in any place on the camera case (see Fig. 4.). Clearly, the measured angular acceleration is $\ddot{\theta}_2$, from which it is possible to recover the angular position.

We report in Fig. 7 the frequency response obtained with spectral analysis methods and limited-bandwidth white noise excitation. Three different types of connection with floor have been considered, namely with high, medium and zero stiffness K_{base} (the latter obtained by using a ball-bearing support). As an expected result, the pole-zero pair at low frequency disappears in case of zero stiffness, with a consequent order reduction in the plant to be controlled. Excluding the latter condition, being not realistic, we can observe that the system shows two evident resonance peaks, which can possibly amplify the torque ripple. With a concrete base, the resonant frequencies are 17.55 Hz and 25.95 Hz, respectively.

It is worth noticing that the reported responses show the relation between stator and load angles.

IV. ACTIVE DAMPING CONTROL DESIGN

In order to design the active damping control, the experimental frequency response has been fitted into the analytical model whose structure is defined in (3). The Bode plot for

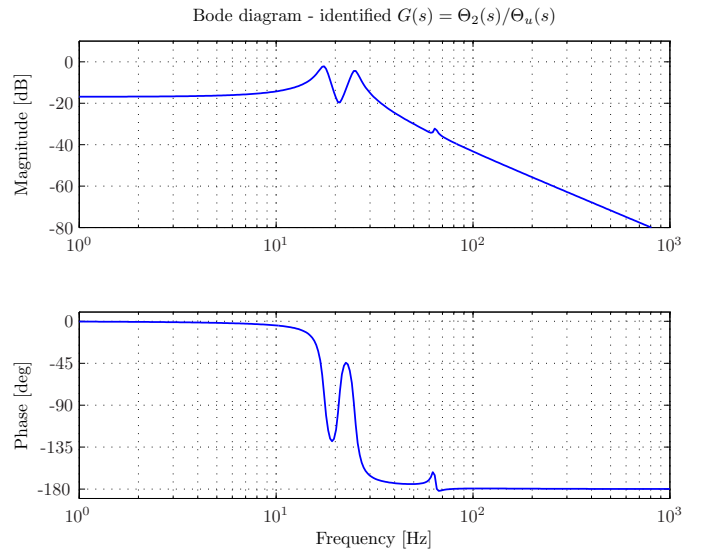


Fig. 8. Fitted Bode plot (by using a frequency-domain least-square fitting procedure) of $\Theta_2(s)/\Theta_u(s)$ in nominal conditions.

nominal plant (concrete base and nominal camera inertia) is shown in Fig. 8. Note that the static gain corresponds to the gear ratio N_G .

All active damping strategies make use of an inner loop, capable of reducing the height of the resonant peaks as well as the oscillations that may be caused by various disturbances. In approaching the design of such inner control, we must consider that there is no precise knowledge about the transfer function, since this may widely change during operation (e.g. when a bird lands on the camera, the load inertia increases and, in turn, all resonance frequencies decrease). An on-line identification procedure, together with an adaptive feedback control scheme could be implemented [12] [13], but this is not compatible with the uninterruptible 24-7 operating scenario of the system considered and the possible sudden large variations in plant parameters. Given the mentioned limitations, we resorted to a simple and robust solution, making use of a load velocity feedback, equivalent to inserting a viscous damper between load and base. This, in turn, is implemented by commanding the actuator to generate a torque proportional to the load vibrational speed, provided that the base is anchored to an inertial reference. This, of course, is an ideal operating condition but it is a realistic approximation of the conditions found in a good camera installation, where the supporting fixtures must not deflect in an appreciable manner during operations.

In order to inject a damping torque in the system hub, we must recall (2), which says that the torque depends linearly on both the phase peak current and the stator flux angle θ_u . While changing the first may require additional energy and possibly a re-design of the current drivers, the second requires only the small variation of the stator flux angle around the standard operating point (i.e. the angle set by the target-following outer loop), under the hypothesis of small differences between stator

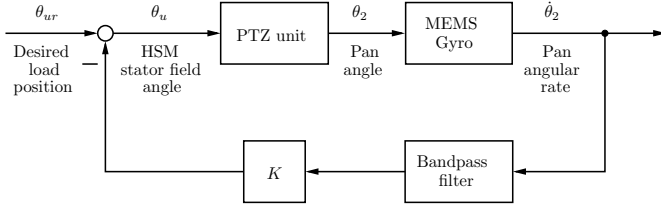


Fig. 9. Active damping inner loop.

and rotor angles. Using this simple consideration, a vibration damping inner loop can be realized in the form shown in Fig. 9, where the load side velocity is obtained by using a MEMS gyroscope (InvenSense IDG1251 x–y axis, with 67 °/s full scale range).

Remarkably, the proposed method to generate a compensating torque in HSM–driven system can be applied also in systems with fixed plant parameters, for which more sophisticated damping schemes can be applied ([13]). In practice, if the target is going to be followed with a constant camera angular speed ω_t , this is achieved by setting the phase currents in the HSM as in (4)–(5), where θ_{ur} represents the desired load position:

$$i_1 = I \cos(\theta_{ur}) = I \cos(\omega_{ur}t) = I \cos(N_r/N_G \omega_t t) \quad (4)$$

$$i_2 = I \sin(\theta_{ur}) = I \sin(\omega_{ur}t) = I \sin(N_r/N_G \omega_t t) \quad (5)$$

When the active damping inner loop is active, the actual angular position for the stator flux is obtained as follows

$$\theta_u = \theta_{ur} - K \dot{\theta}_2 \quad (6)$$

i.e. by subtracting a signal proportional to the load angular velocity to the reference angle θ_{ur} . This, as shown above, is equivalent to ask to the HSM to generate a torque proportional to the load angular velocity, as required by the active damping strategy. It is worth noticing that the actual implementation of the inner loop must take into account that the MEMS gyroscope may have some bias and high frequency noise in its output, so a band–pass filter must be placed in the feedback path of the control scheme in Fig. 9. This, additionally, avoids a constant displacement between set–point and actual rotor position that would appear when operating at constant angular speed.

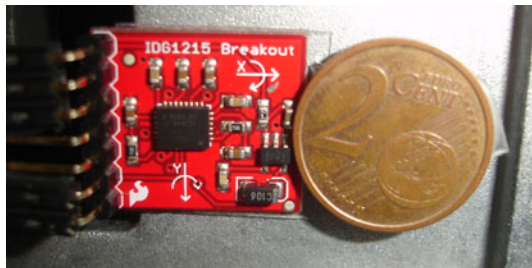


Fig. 10. MEMS gyroscope placed inside the unit.

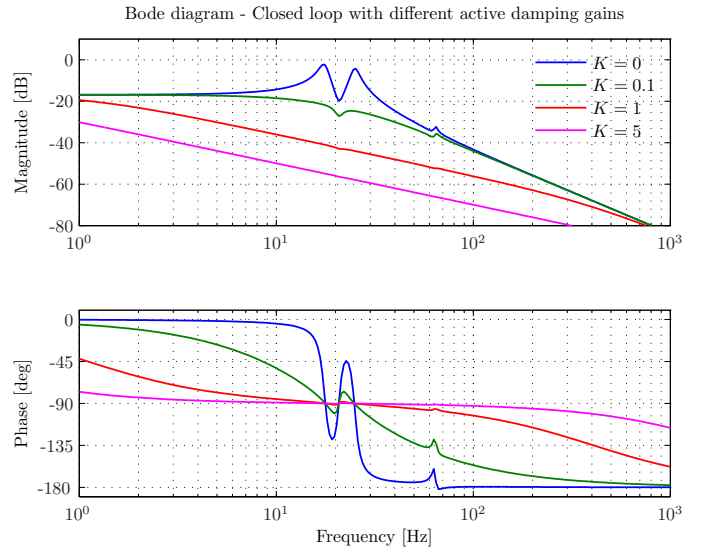


Fig. 11. Input/output frequency response with different compensation gains.

The design of the inner loop clearly reduces to the choice of the feedback gain K . Actually, if the damping of the resonant modes is the control objective, a high value of K would lead to better results, as shown in Fig. 11.

On the other hand, this choice leads to a problem, because the amplitude of the compensation signal may become larger than a quarter of the HSM step width, and this may cause the rotor of the HSM to fail to follow the reference profile. For this reason, the best value of the compensation gain should be found experimentally.

V. EXPERIMENTAL RESULTS

The active damping control presented in the previous section has been applied to the camera positioning unit and its effectiveness proven in different operating conditions. Fig. 12 shows the comparison of the spectra of the load vibrations, measured by the MEMS gyroscope, with and without the active damping. The band–pass filter has been designed in order to introduce the least phase delay around the first resonant frequency and has a flat response between 1 and 100 Hz . The rotating speed of the hub is chosen so that the first

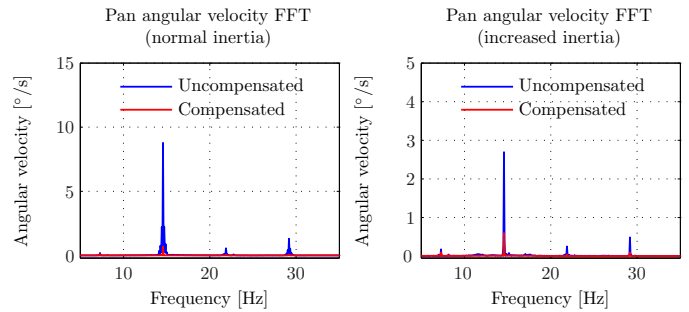


Fig. 12. Vibration attenuation with different load inertia (nominal on the left, doubled on the right) – constant speed test (hub angular velocity = 15°/s).

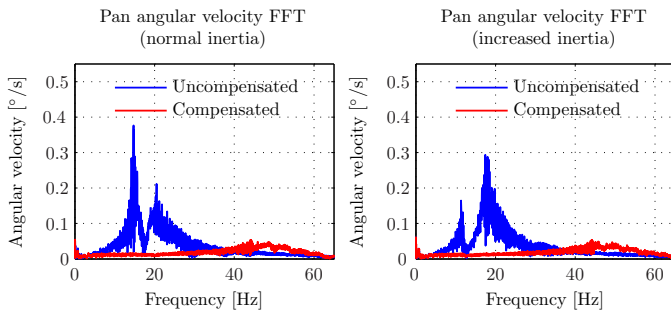


Fig. 13. Vibration attenuation with different load inertia (nominal on the left, doubled on the right) – constant acceleration test (hub angular acceleration reference = $1.25^\circ/s^2$)

harmonic of the HSM torque ripple falls in the resonant peak of the frequency response (i.e. $15^\circ/s$ in the unit under test – this value is well within the pan speed operating range of the unit, which is stated to be equal to $0.02^\circ/s \div 100^\circ/s$). As a result, a reduction of 95% of the vibration amplitude is achieved, even in case of a large variation of the load inertia, obtained by placing an additional weight on top of the camera.

The robustness against load inertia variations has been verified, also in variable speed operating scenario. The results shown in Fig. 13 report the vibrations measured when the system operates at constant angular acceleration (hub angular acceleration reference = $1.25^\circ/s^2$) and they confirm the effectiveness of the proposed control scheme and its insensitivity to wide changes in operating conditions.

The results obtained with the use of a load-side MEMS gyroscope are essentially comparable with those reported in [1] and obtained with a MEMS accelerometer placed on the unit. It is worth noticing that in the second case, the amplitude of the measured tangential acceleration (and, in turn, of the angular speed) depends on the position of the sensor w.r.t. the pan axis. On the other hand, the gyroscope can be placed anywhere on the system, giving more freedom in the design. As for the level of performance achieved, for the sensors used here, the MEMS accelerometer shows a better noise figure, which allows the achievement of a more effective compensation. Comparisons on this specific aspect will be reported in the final version of the paper.

VI. CONCLUSIONS

Active damping control is widely adopted for reducing the vibrations in motion control systems. This technique, however, has been used so far only in those systems provided with a torque-controlled actuator. The reported application shows how it is possible to extend the application of this method even to motion control systems driven by HSM. The proposed solution can be easily retrofitted on existing hardware, being based on the use of load-side MEMS gyroscope and a simple modification of the microstepping technique. Experimental results show the robustness and effectiveness of a simple load velocity feedback in suppressing vibrations. The method developed for driving the HSM in order to produce a compensation

torque can be applied to other mechatronic systems and its use in conjunction with more complex control schemes, possibly adaptive, will be the subject of future research.

ACKNOWLEDGMENT

This work has been partially supported by the Programma Operativo F.S.E. 2007-2013 Regione Veneto, Codice Progetto 2105/101/17/2214/2009 (“Modellizzazione Orientata al Controllo di Sistemi Meccatronici”). Authors would like also to thank Videotec (Schio, Vicenza, Italy) for providing (and allowing to hack) the camera positioning unit. Thanks go also to Enrico Zambon for his valuable contribution to the experimental activity.

REFERENCES

- [1] R. Antonello, A. Cenedese, and R. Oboe, “Active damping applied to hsm-driven mechanical loads with elasticity,” in *Proc. 18th World Congress of the International Federation of Automatic Control (IFAC)*, Aug. 2011.
- [2] T. Kenjo, *Stepping Motors and Their Microprocessor Controls*. Oxford: Clarendon Press, 1984.
- [3] M. Rahman and C. Grantham, “Design approaches for microstepping step motor controllers,” in *Power Electronics and Variable-Speed Drives, 1991., Fourth International Conference on*, jul. 1990, pp. 253–257.
- [4] H.-S. Ahn, Y. Chen, and H. Dou, “State-periodic adaptive compensation of cogging and Coulomb friction in permanent magnet linear motors,” in *American Control Conference, 2005. Proceedings of the 2005*, jun. 2005, pp. 3036–3041 vol. 5.
- [5] M. Bodson, J. Chiasson, R. Novotnak, and R. Rekowski, “High-performance nonlinear feedback control of a permanent magnet stepper motor,” *Control Systems Technology, IEEE Transactions on*, vol. 1, no. 1, pp. 5–14, mar. 1993.
- [6] A. Blauch, M. Bodson, and J. Chiasson, “High-speed parameter estimation of stepper motors,” *Control Systems Technology, IEEE Transactions on*, vol. 1, no. 4, pp. 270–279, dec. 1993.
- [7] D. Kos, A. Kapun, M. Curkovic, and K. Jezernik, “Efficient stepper motor torque ripple minimization based on fpga hardware implementation,” in *IEEE Industrial Electronics, IECON 2006 - 32nd Annual Conference on*, nov. 2006, pp. 3916–3921.
- [8] J. E. McInroy, R. M. Lofthus, and S. A. Schweid, “Step motor supply: Minimizing torque ripple induced by digital linearization,” *Control Engineering Practice*, vol. 3, no. 9, pp. 1225–1235, 1995.
- [9] D. Miu, *Mechatronics*. New York: Springer Verlag, 1993.
- [10] L. Bascetta, P. Rocco, and G. Magnani, “Force ripple compensation in linear motors based on closed-loop position-dependent identification,” *Mechatronics, IEEE/ASME Transactions on*, vol. 15, no. 3, pp. 349–359, jun. 2010.
- [11] R. Antonello, A. Cenedese, and R. Oboe, “Torque ripple minimization in hybrid stepper motors using acceleration measurements,” in *Proc. 18th World Congress of the International Federation of Automatic Control (IFAC)*, Aug. 2011.
- [12] C.-C. Wang and M. Tomizuka, “Sensor-based controller tuning of indirect drive trains,” in *Advanced Motion Control, 2008. AMC '08. 10th IEEE International Workshop on*, mar. 2008, pp. 188–193.
- [13] C.-H. Han, C.-C. Wang, and M. Tomizuka, “Suppression of vibration due to transmission error of harmonic drives using peak filter with acceleration feedback,” in *Advanced Motion Control, 2008. AMC '08. 10th IEEE International Workshop on*, mar. 2008, pp. 182–187.